1. Agency Use	2. Report Date.	3. Report Type and Dates Covered.
	1994	Final - Journal Article

4. Title and Subtitle.
The Partition Wavenumber in Acoustic Backscattering from a Two-Scale Rough Surface Described by a Power-Law Spectrum

5. Funding Numbers.

Program Element No.	0601153N
Project No.	3204
Task No.	040
Accession No.	DN251004
Work Unit No.	571520603

6. Author(s).
Caruthers, J. (2nd) and J. Novarini (1st)*

7. Performing Organization Name(s) and Address(es).
Naval Research Laboratory
Ocean Acoustics Branch
Stennis Space Center, MS 39529-5004

8. Performing Organization Report Number.
IEEE Journal of Oceanic Engineering, Vol. 19, No. 2, April 1994, pp. 200-207

9. Sponsoring/Monitoring Agency Name(s) and Address(es).
Office of Naval Research
800 N. Quincy St.
Arlington, VA 22217-5000

10. Sponsoring/Monitoring Agency Report Number.
NRL/JA/7175--93-0016

11. Supplementary Notes.
*Planning Systems Inc.
Slidell, LA 70458

12a. Distribution/Availability Statement.
Approved for public release; distribution is unlimited.

12b. Distribution Code.

13. Abstract *(Maximum 200 words).*

Scattering from the ocean bottom is often assumed to be controlled by two spatial scales: the larger scale associated with reflections from plane facets, and the smaller one associated with diffuse scattering from height variations. Choosing the wavenumber for this partitioning has proven to be important but troublesome. For this work, scattering data are simulated using Helmholtz-Kirchhoff or physical optics theory and selected input geomorphology. These data are inverted to provide rms slope of facets and rms heights of small-scale roughness using a simple two-scale roughness model introduced recently (J.W. Caruthers and J.C. Novarini, *IEEE J. Oceanic Eng.*, vol. 18, pp. 100-106, 1993). Bottom relief is described by power spectra of the power law form, and the bottom is assumed to be impenetrable. The work introduces a new criterion for effecting this partition based on setting a roughness parameter equal to unity. The criterion is shown to be valid for the cases analyzed based on the ability of the inversion model to recover the input geomorphology.

14. Subject Terms.
Bottom scattering; reverberation

15. Number of Pages.
8

16. Price Code.

17. Security Classification of Report.	18. Security Classification of This Page.	19. Security Classification of Abstract.	20. Limitation of Abstract.
Unclassified	Unclassified	Unclassified	SAR

The Partition Wavenumber in Acoustic Backscattering from a Two-Scale Rough Surface Described by a Power-Law Spectrum

Jorge C. Novarini and Jerald W. Caruthers

Abstract—**Scattering from the ocean bottom is often assumed to be controlled by two spatial scales: the larger scale associated with reflections from plane facets, and the smaller one associated with diffuse scattering from height variations. Choosing the wavenumber for this partitioning has proven to be important but troublesome. For this work, scattering data are simulated using Helmholtz–Kirchhoff or physical optics theory and selected input geomorphology. These data are inverted to provide rms slope of facets and rms heights of small-scale roughness using a simple two-scale roughness model introduced recently (J. W. Caruthers and J. C. Novarini, *IEEE J. Oceanic Eng.*, vol. 18, pp. 100–106, 1993). Bottom relief is described by power spectra of the power law form, and the bottom is assumed to be impenetrable. The work introduces a new criterion for effecting this partition based on setting a roughness parameter equal to unity. The criterion is shown to be valid for the cases analyzed based on the ability of the inversion model to recover the input geomorphology.**

I. Introduction

THE two-scales roughness theory, also called the composite-roughness theory, is particularly attractive because it separates scattering into what appears to be its two primary mechanisms: scattering controlled by large random facets, and scattering controlled by smaller scale roughness. The reported advantage of this approach is that its applicability can span a wide range of surface roughness since it allows for the selective application of appropriate approximations in scattering theory. While this is certainly true, it leads one to attempt to answer the troublesome question of where to set the scale partition based on the requirement for the validity of the approximations. The question should rather be posed in terms of: "At which scales is the scattering-like reflection from a collection of facets and at which scales is the scattering-like diffraction from roughness?."

The two-scale roughness (TSR) approach was first proposed by Kur'yanov [1] and further developed and extended by McDaniel [2]. In its original formulation and in most of its applications [1]–[3], TSR scattering models resort to a combination of the Helmholtz–Kirchhoff or physical optics theory, which is used to describe scattering from the large-scale surface, with a Rayleigh–Rice perturbation method to account for scattering at the small-scale roughness. McDaniel [4] later developed a TSR scattering model based entirely on the Kirchhoff approximation, and derived a diffractive correction to relax the effects of the selection of the partition wavenumber of the surface spectrum. Other TSR approaches, of a heuristic nature, that allow for a rapid estimation of the scattering strength of a rough surface are found in the literature. Among them are Brekovskikh and Lysanov [5] for scattering from the sea surface, and Martin [6] and Ellis and Growe [7] for scattering from the seafloor.

Manuscript received September 1992; revised June 1993. This work was supported by the Acoustic Reverberation Special Research Project of the Office of Naval Research.

J. C. Novarini is with Planning Systems Inc., Slidell, LA. 70458 USA.

J. W. Caruthers is with the Naval Research Laboratory, Stennis Space Center, MS 39529 USA.

IEEE Log Number 9216757.

II. Applicable Scattering Models

In this work, we deal with a TSR model originally developed for bistatic bottom scattering strength calculations for wide area applications [8], the bistatic scattering strength model (BISSM). An upgrade of the forward scattering calculation of the algorithm has been recently reported [9]. The term BISSM has been applied to a collection of programs for the prediction of the scattering strength and reverberation from the seafloor. Here, we introduce the term rough facet model (RFM) to refer to that part of BISSM that is the mathematical description of the scattering mechanisms.

The application of the rough facet model to sidescan sonar images, as well as preliminary applications to the inverse problem have been reported elsewhere [10], [11]. The attention of this work will be focused on the partition wavenumber. The ultimate goal is to allow the scattering phenomenon itself to suggest what should be the scale partition. RFM allows inversion of the scattering problem, and thereby the extraction of slope and height roughness for the scattering surfaces. Since no reliable experimental data are available (there is a lack of scattering measurements accompanied by a detailed description of the bottom roughness at the appropriate scales), scattering data are simulated using a high-fidelity, 2-D scattering model and selected input seafloor morphology. This high-fidelity model, which we refer to as the benchmark or groundtruth model, is based on Monte Carlo evaluation of the Helmholtz–Kirchhoff (H/K) integral over an ensemble of surfaces with the desired statistical properties. RFM predictions are fitted to results from the H/K simulations, and the scale partition is established when recovery of the correct geomorphology is accomplished.

A. The Rough Facet Model

The RFM algorithm predicts the bistatic scattering strength of a directional 2-D seafloor for arbitrary source/receiver directions. Here, it is applied to monostatic scattering from 2-D isotropic surfaces. It resorts to the TSR concept in the sense that the problem of scattering from a multiscale rough surface is approximated by separating the scattering problem into fine-scale and microscale roughness (microroughness) effects. Large-scale roughness, associated with long surface wavelengths present in standard bathymetric databases, are handled deterministically and are excluded from this analysis. That is, we consider here only the roughness within the footprint of ensonification, and assume that any tilt of the seafloor under this footprint can be removed deterministically.

The scattering coefficient is decomposed into two components: one (component m_1) mainly controlled by diffuse scatter in the incoherent field, and the other (component m_2) mainly controlled by a facet reflection process which for individual facets is partially coherent, but collectively incoherent. Accordingly, the total bistatic scattering strength is given by

$$m_{bs} = m_1 + m_2. \tag{1}$$

The adopted methodology is somewhat similar to the treatment followed by Brekovskikh and Lysanov [5] and Martin [6] (referred to as "standard" here), in which the m_1 and m_2 correspond to the micro- and fine-scale components, respectively. However, unlike all previous work, the m_2 term in RFM contains information on microroughness as well as fine-scale slopes. That is, the major distinction between FRM and the standard model is the distinction between rough facets and flat, smooth facets. It is important to recognize that for a random distribution of flat, smooth facets (a broken mirror), each facet reflects coherently; incoherence is introduced by the statistical sum over the distribution. In the standard treatment, as well as in the methodology adopted here, wide-angle scatter is produced by m_1. The fine-scale surface gives rise to the near-specularly scattered lobe described by m_2. In contrast to the standard treatment, however, microroughness also contributes to additional loss in the specular lobe, and provides a correction to account for diffractive loss in RFM in the near-specular direction.

The incoherent component is based on Lambert's law. It would usually include an empirically determined coefficient such as Mackenzie's coefficient [12]. This term, however, is ignored here because we limit our attention to the near-specular direction, that is, in the monostatic case, near normal. On the other hand, the facet scatter part, which constitutes the major scattering component in the specular lobe, is the most sensitive to the partition wavenumber. We, therefore, focus our attention on m_2.

The additional coherence or scattering loss at each facet in the RFM is accounted for in m_2 with a multiplicative factor. This factor was chosen to be the so-called "coherent-reflection coefficient," originally derived by Eckart in the framework of an H/K formalism [13]. It accounts for the low-frequency (i.e., small-scale) scattering by the microroughness in the local specular direction. (By "specular direction," in general we mean the direction a ray would reflect from a hypothetical flat mean plane substituted for the scattering patch. The additional modifier "local" designates the specular direction of an individual fine-scale facet.) Therefore, in the RFM, the m_2 component of the scattering coefficient reduces to

$$m_2 = M(k, \sigma_\mu, \Theta) \cdot F(\delta_f, \Theta) \tag{2}$$

where $M(\cdot)$ is the contribution of the microroughness and $F(\cdot)$ is the contribution of the fine-scale slopes. The additional parameters are: k, the acoustic wavenumber; σ_μ, the standard deviation of the microroughness; δ_f, the standard deviation of the fine-scale slopes; and Θ, the angle of incidence measured from normal (zenith angle). (We also define the slope angle $\alpha_f = \tan^{-1}\delta_f$.) For the developments of $M(\cdot)$ and $F(\cdot)$, Gaussian height and Gaussian slope distributions are assumed, respectively.

The coherent reflection coefficient is given by

$$M = \exp[-g_\mu] \tag{3}$$

where g is the well-known roughness parameter [14] restricted here to the microroughness, i.e.,

$$g_\mu = 4\sigma_\mu^2 k^2 \cos^2\Theta. \tag{4}$$

The function $F(\cdot)$ is the high-frequency limit of the H/K theory as derived by Eckart [13], Beckman and Spizzichino [14], and Brekhovskikh and Lysanov [5]. (The form adopted here is identical to that of [5].) For the present application, $F(\cdot)$ reduces to

$$F = \frac{R_0^2}{8\pi\delta_f^2\cos^4\Theta}\exp\left[-\frac{\tan^2\Theta}{2\delta_f^2}\right] \tag{5}$$

where R_0 is the Rayleigh reflection coefficient. For this work, $R_0 = 1$.

In [9], we introduced RFM in a heuristic manner. Here, in the Appendix, we provide a more formal theoretical foundation for the model.

B. The Benchmark Model

As a benchmark, we adopt here a model which consists of numerically evaluating the full Helmholtz–Kirchhoff integral with a minimum number of approximations. A complete description of the technique can be found in [15]. The complex scattered field for a point source and a 2-D surface is calculated. No Fraunhofer or Fresnel approximation is invoked, and the full wavefront curvature is kept in the calculations. The complex pressure at the point $\boldsymbol{r}$ is given by

$$p(\boldsymbol{r}) = \frac{ik}{4\pi}\int_{S'} D(x', y') \frac{\exp[ik(R_1 + R_2)]}{R_1 \cdot R_2}\left(\frac{\boldsymbol{R}_1}{R_1} - \frac{\boldsymbol{R}_2}{R_2}\right)\cdot \boldsymbol{n}\, dS' \tag{6}$$

where $\boldsymbol{R}_1 = \boldsymbol{r}' - \boldsymbol{R}_{\text{source}}$ and $\boldsymbol{R}_2 = \boldsymbol{R}_{\text{receiver}} - \boldsymbol{r}'$, and $\boldsymbol{r}'$ is the position vector of a point on the random surface. The integration indicated is over the 2-D scattering surface S', and $\boldsymbol{n}$ is

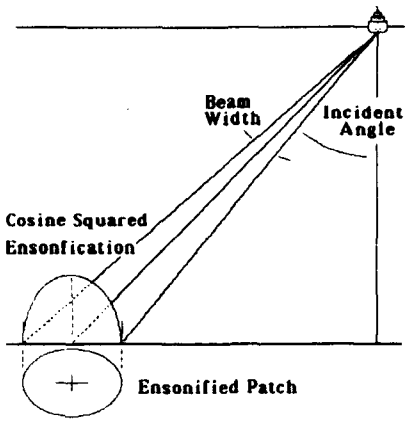

Fig. 1. Geometry of the simulated scattering experiments.

the normal to the surface element dS'. The function $D(x, y)$ represents the ensonification function over the surface. Here, for the monostatic case, $|\boldsymbol{R}_{\text{source}}| = |\boldsymbol{R}_{\text{receiver}}| = R$.

There are two advantages for using this model as groundtruth: the H/K formalism has been shown to be highly accurate in predicting near-specular scattering from multiscale surfaces [16], and the RFM model is based entirely on the H/K approximation.

III. Numerical Simulations

Although this is a purely numerical study, a practical scenario based on a high-frequency multibeam, swath bathymetric sonar system is adopted here because it will allow easy testing of the results, and because we envision that system as a major application of these results once they are validated. However, the scenario is also applicable to the low-frequency active sonar system used in the Acoustic Reverberation Special Research Program (ARSRP) of the Office of Naval Research (ONR). Data taken during a recent experiment of the ARSRP will be useful in future validations of results obtained here. In particular, the lowest frequency (250 Hz) chosen here is applicable specifically to that data. The highest frequency (2 kHz), while still lower than the range of standard shipborne multibeam sonars, is within the range of new or planned towed swath systems that incorporate both sidescan imaging and bathymetric capabilities.

A. Description of the Numerical Experiments

Fig. 1 illustrates the geometry of the simulated experiment. Shown in the figure is the representation of a typical transverse beam of the multibeam sonar. The water depth is chosen to be 2000 m and the beamwidth is 2°. Zenith angles are set at 3–43° in 2° increments. Four acoustic frequencies are investigated: 250 Hz, 500 Hz, 1 kHz, and 2 kHz. A constant velocity of 1500 m/s is assumed. The use of an isovelocity sound velocity profile is not a problem for the near-vertical angles used in the study.

For each ensonified region, the pressure was calculated from (6) assuming a cosine-squared ensonification function to minimize sidelobes; the scattered intensity is then obtained as the ensemble average of pp^* over the ensemble of subregions. The backscattering coefficient is defined as

$$\text{BSS} = 10\log\left(\langle pp^*\rangle R^2/AI_i\right)) \tag{7}$$

where A is the area of the ensonified region (weighted by the ensonification pattern) and I_i $(= p_s^2/R^2)$ is the incident intensity. We normalize the source pressure (p_s) at 1 m to 1 μPa.

B. Simulated Two-Dimensional Surfaces

Ensembles of 2-D (i.e., surface heights are functions of x and y) randomly rough surfaces were generated using a filtering technique developed by Caruthers and Novarini [17], [18]. This technique consists of smoothing a 2-D array of uncorrelated random numbers with a filter whose transfer function is proportional to the square root of the power spectrum of the surface elevations. The amplitude spectrum that is most often used to describe seafloor roughness is of the power-law form

$$A(K) = aK^{-b} \tag{8}$$

and the surfaces are assumed to be isotropic. K is the wavenumber of the surface roughness (in cycles/meters). Note that the corresponding power spectrum is $W(K) = a^2K^{-2b}$.

It should be noted that, in the RFM scattering model, the two surface parameters (the rms height of the microscale surface and the rms slope of the fine-scale surface) are band-limited quantities. The variance of the microroughness for a 2-D isotropic surfaces is given by

$$\sigma_\mu^2 = 2\pi\int_{K_c}^{K_h} W(K)K\,dK. \tag{9}$$

The variance of the slopes of the fine-scale surface is given by

$$\delta_f^2 = 2\pi\int_{K_l}^{K_c} W(K)K^3\,dK. \tag{10}$$

In (9) and (10), K_l and K_h indicate the low- and high-frequency wavenumbers present on the surface, respectively. These wavenumbers are determined by the size of the footprint and the grid spacing, respectively. K_c denotes the partition (cutoff) wavenumber. When the partition wavenumber is allowed to be frequency dependent, then both σ_μ^2 and δ_f^2 are functions of the acoustic frequency. This point is made to draw attention to the fact that $F(\cdot)$ of (5) is frequency dependent, contrary to the usual presumption.

Table I shows the spectral parameters a and b for the surfaces used in this work. Given in the table are σ_T, the total rms height (i.e., allowing all the deformation of the surface to be microroughness) and δ_T, the total rms slope (i.e., allowing all the deformation of the surface to be slope variance). Also given in the table is the slope angle α_T. The dimensions for each of the surfaces is 256 × 256 m (1024 × 1024 grid points, with a grid spacing of 0.25 m). The grid spacing of 0.25 m bounded the analysis in frequency and angle to 2 kHz and 43°, respectively, owing to the existence of grid resonances

TABLE I
PARAMETERS OF THE POWER-LAW SPECTRA FOR THE SIMULATED SURFACES

Surface Label	Spectral Paraameters a (m^2)	b	rms values δ_T	δ_T	α_T (deg)
OF	2.32×10^{-2}	1.75	1.80	0.594	30.7
O1	1.86×10^{-2}	1.75	1.45	0.477	25.5
OD	6.00×10^{-3}	2.27	4.47	0.464	24.9
OI	4.80×10^{-3}	2.27	3.58	0.372	20.4
OJ	3.0×10^{-3}	2.27	2.24	0.233	13.1

beyond these limits. For Kirchhoff validity, however, we will not attempt to fit data beyond 35°.

Each surface realization was split into a number of ensonified regions (sonar footprints) for ensemble averaging purposes. The number of subregions depends on the geometry of the simulation and the zenith angle of incidence, and varies between 9 to 2 as the angle varies between 3 and 43°.

IV. RESULTS

To investigate the spectral partition, predictions from the RFM model were fitted to the simulated data from the groundtruth H/K model. These fits established values for σ_μ and δ_f which were required to be consistent with the simulated surface geomorphology and were constrained by (9) and (10). Success was achieved when a value of K_c could be established that satisfied the constraints. As mentioned earlier, the partition wavenumber is usually established based on either the formal limits of the approximations invoked [19] or upon a partition factor that is the ratio of the partition wavelength for the surface L_c to the acoustic wavelength l_a, that is, $x = L_c/l_a$ [20]. The cutoff wavenumber is, therefore, $K_c = k/(2\pi x)$.

Here, we hypothesize that the scattering phenomenon itself will establish a facet size such that the microroughness that exists upon it leads to $g_\mu \approx 1$. Larger regions contain too much roughness to produce a coherent facet reflection and, therefore, cannot be a facet. Smaller regions are not the full extent of a facet that can cause a coherent reflection. Therefore, the partition wavenumber can be determined from (4) and (9) and δ_f determined from (10).

For simplicity, we will approximate g_μ for all angles (0–43°) by its value at $\Theta = 0°$, i.e., $g_{\mu 0} = 4\sigma_\mu^2 k^2 \approx 1$. This could lead to some error at the wider angles. However, we do not press the issue for precision because other sources of error exist at the wider angles. The sources of error at wide angles will be discussed in the next several paragraphs as we quantify the amount of error.

Adopting the aforementioned criterion (i.e., to assume that $g_{\mu 0} = 1$ and determine the resulting K_c and δ_f), we proceed to compare the scattered field from surface $0D$ ($b = 2.27$) at 500 Hz, with predictions from the RFM. Fig. 2(a) illustrates the effect in (2) and (5) of varying the slope of the spectrum (b) in computing δ_f from (10). Note, first, that for this case, scattering described by RFM is strongly dependent on the spectrum slope. And second, the best agreement occurs at about $b_{est} = 2.14$. This departure from the expected $b = 2.27$ is not particularly troublesome because spectral analysis

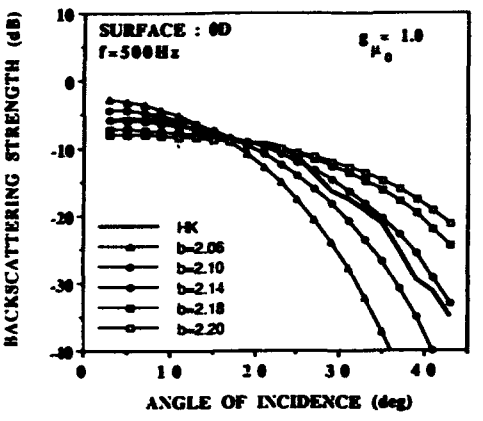

(a)

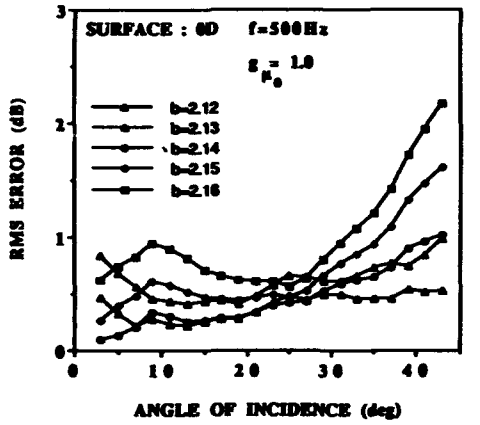

(b)

Fig. 2. Comparisons of the RFM and H/K model results at 500 Hz for surface 0D for different values of spectral slope b assuming that $g_{\mu o}$=1: (a) Backscattering strength; (b) RMS error.

of the actual surface realizations resulted in an estimate of spectral slope that had uncertainty limits of 2.10 and 2.35. For practical reasons, the surface spectral slopes were estimated from the overall surfaces rather than averages over the ensonified footprints extracted from them.

To allow for a more detailed examination of the agreement, we establish an error parameter. To that end, we integrate the difference in decibels from normal incidence out to some angle Θ_n and divide by Θ_n to get the average error out to that angle. In digital form, this becomes

$$E = 1/N * \mathrm{SUM}[\mathrm{abs}(\mathrm{BSS_{RFM}} - \mathrm{BSS_{HK}})](\mathrm{dB}) \qquad (11)$$

which provides an error measure from normal to the angular bin N.

We examine the results in Fig. 2(a) more closely by applying (11) and display these details in Fig. 2(b). Note that the average error is increasing with angle from normal, but for $b_{est} = 2.14$, the average error remains below 0.5 dB. It might be noted that the point errors do not exceed 4 dB, even for losses of 33 dB. To determine if we can fine-tune the value of $g_{\mu 0}$, Fig. 3 displays the error parameter versus angle for $b_{est} = 2.14$ and with $g_{\mu 0}$ varying. We find that, in this case, $g_{\mu 0} = 1.0$ appears to be the best choice to two significant figures.

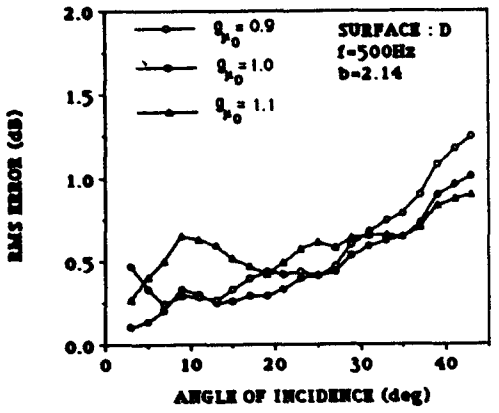

Fig. 3. RMS error between RFM and H/K model results for surface 0D for an iteration on the roughness parameter of the micro-scale surface having established the spectral slope at b_{est}=2.14 as the best fit for $g_{\mu o}$.

TABLE II
BANDLIMITED RMS ROUGHNESS FOR SURFACE OD FOR $g_{\nu o}$=1 CORRESPONDING TO THE BEST FITTING PARAMETERS a=6.10^{-3} AND b_{est}=2.14

	250 Hz	500 Hz	1 kHz	2 kHz
σ_μ(m)	0.47	0.23	0.12	0.06
α_f (deg)	11.5	13.1	14.3	15.3
x	4.9	5.4	5.9	6.4

Fig. 2(b) and 3, as well as others to be seen later, show errors beginning to appear at wider angles. Clearly, the basic assumptions of near-specular scattering are breaking down, and we introduced an obvious error by using $g_{\mu 0}$ instead of g_μ, but there are other sources of error introduced by practical constraints on the simulation. These include: 1) at the lower frequencies, errors are introduced by diffraction at the edges of the ensonified region; 2) at the higher frequencies, errors are introduced by grid resonances; and 3) statistical errors introduce the limited number of surface realizations (nine near normal, two near 43°—although not as bad as it appears since there are many correlation lengths in the surfaces and there are more at wider angles). In spite of these sources of error, the results are very good out to 35° and beyond in some cases.

To test the robustness of the criterion, the RFM was run for the same surface, $0D$, at three other frequencies (250 Hz, 1 kHz, and 2 kHz). In each case, there is a narrow range of b values that agree with the H/K curve within 3 dB. The value b_{est} = 2.14 obtained for 500 Hz turned out to be a good compromise for the four frequencies. Fig. 4(a)–(c) shows the agreement. The matching between the RFM prediction and the groundtruth model is excellent. Table II gives the rms height of the microroughness and the rms slope angle of the fine-scale component for each frequency. Also shown is the partition factor x. Notice that x varies significantly and consistently over the three octaves.

The same procedure of looking for the spectral parameter b that leads to the best agreement for $g_{\mu 0}$ = 1.0 was repeated for surface $0F$ at 250 Hz. (Note that surface $0F$ has a significantly different total variance of height and only a small difference in total slope variance from surface $0D$.) The best agreement (b_{est} = 1.75) was found at the expected value of b = 1.75. In Fig. 5, the effect of changing $g_{\mu 0}$ is shown for surface

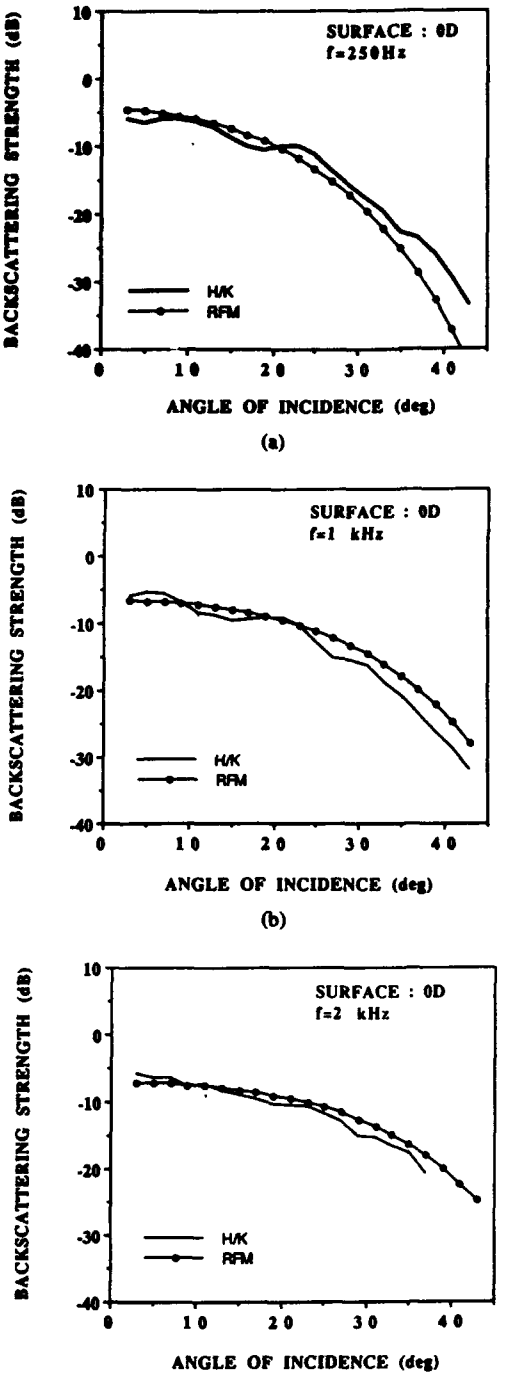

Fig. 4. Comparisons of the RFM and H/K model results for surface 0D for various frequencies having adopted b_{est}=2.14 and $g_{\mu o}$=1: (a) 250 Hz.; (b) 1 kHz; and (c) 2 kHz.

$0F$. As happened for surface $0D$, the output of RFM is quite sensitive to changes in $g_{\mu 0}$. Again, the best agreement occurs at $g_{\mu 0}$ = 1.0. Table III lists the band-limited roughness for surfaces $0D$ and $0F$, at 250 Hz, for different $g_{\mu 0}$. The partition factors (x) are also shown. It can be seen that x corresponding to the best agreement ($g_{\mu 0}$ = 1.0) is markedly different in the two cases. This indicates that the number of acoustic wavelengths cannot *per se* provide a criterion to determine the partition wavenumber.

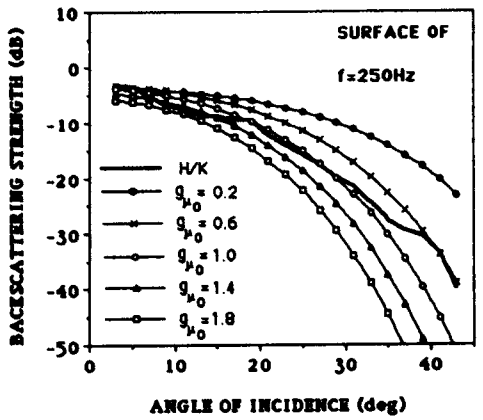

Fig. 5. Comparisons of RFM and H/K model results for surface OF for an iteration on the roughness parameter of the micro-scale surface having established the spectral slope at b_{est}=1.75 as the best fit for $g_{\mu o}$=1.

TABLE III
BANDLIMITED RMS MICROROUGHNESS FOR f=250 Hz FOR NUMERICAL REALIZATIONS OF SURFACES OF (b_{est}=1.75) AND OD (b_{est}=2.14)

	SURFACE OF			SURFACE OD		
$g_{\mu o}$	x	σ_μ(m)	α_f(deg)	x	σ_μ(m)	α_f(deg)
0.2	1.2	0.21	15.5	2.4	0.21	13.3
0.6	2.5	0.37	12.1	3.9	0.37	12.2
1.0	3.6	0.47	10.6	4.9	0.47	11.5
1.4	4.4	0.56	9.6	5.7	0.56	11.0
1.8	5.3	0.64	8.9	6.4	0.64	10.6

To further test the robustness of the proposed criterion for the partition wavenumber to decreasing roughness, the model was applied to a family of surfaces (surface $0I$ and $0J$) that were generated from surface $0D$ by reducing the surface parameter a (i.e., decreasing the spectral amplitude while keeping the spectral slope b constant). Results are shown in Fig. 6 for a frequency of 250 Hz. Table IV shows the rms values of the fine-scale slope angle and the rms height of the microroughness in each case. In all cases, the criterion $g_{\mu 0} = 1.0$ leads to the best agreement.

As a final application, the method was applied to a surface having a spectrum of the type describing the ARSRP reconnaissance area [18]. The surface is labeled 01. The spectral parameters are listed in Table I. The acoustic frequency is 250 Hz, and the partition wavenumber was determined according to the proposed criterion $g_{\mu 0} = 1$. Fig. 7 shows the best agreement with the RFM. It was achieved for $b_{est} = 1.85$, i.e., 5% off the theoretical value of 1.75. This discrepancy is well within the error in the spectral slope of the surface realizations. The resulting microroughness (σ_μ) is 0.47 m and the rms slope angle (α_f) is 12.3°.

V. CONCLUSIONS

The partition wavenumber between the two scales of roughness in composite-surface scattering theory for surfaces having power-law spectra, typical of the seafloor, has been investigated through numerical simulation. Results indicate that a criterion based on the smoothness of the microscale component

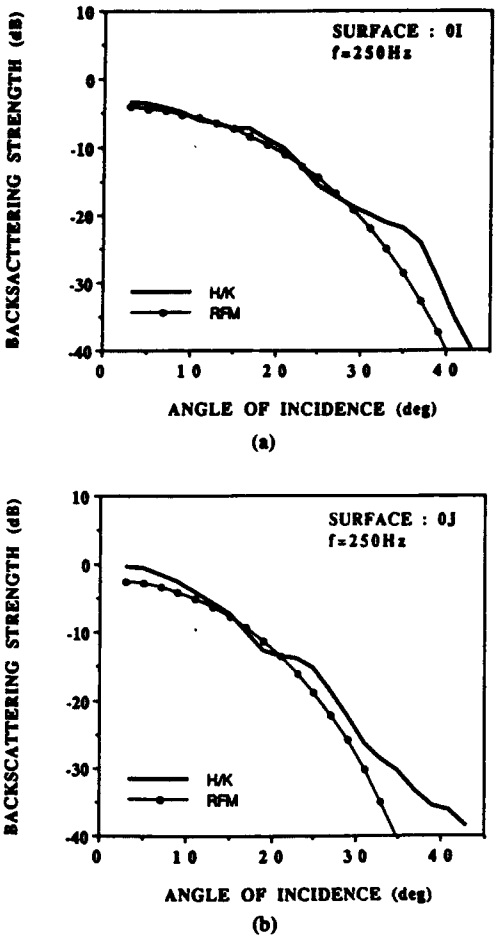

Fig. 6. Comparisons of RFM and H/K model results for (a) surface OI (b_{est}=2.18) and (b) surface OJ (b_{est}=2.26) for the best fit at $g_{\mu o}$=1.

TABLE IV
BEST FIT PARAMETERS AND BANDLIMITED RMS MICROROUGHNESS FOR SURFACES WITH DIFFERENT DEGREES OF ROUGHNESS AT A CONSTANT FREQUENCY OF250 Hz (CUTOFF CRITERION: $g_{\nu o}$=1)

surface label	spectral parameters a (m^2)	b_{est}	band-ltd rms values σ_μ	α_f (deg)	partition x
OF	2.3×10^{2}	1.75	0.47	10.3	3.6
01	1.9×10^{2}	1.85	0.47	12.3	3.5
OD	6.0×10^{3}	2.14	0.47	11.5	4.9
OI	4.8×10^{-3}	2.18	0.47	10.6	5.4
OJ	3.0×10^{-3}	2.26	0.47	8.9	7.5

may be adequate to establish the partition. We find that the partition wavenumber appears to be set by the physics of scattering to be $g_{\mu 0} = 1.0$ within two significant figures.

We introduce the hypothesis that a facet will be formed such that its roughness is approaching a value that begins to destroy the coherence of scatter from the facet. Larger facets are not allowed because coherent reflection is not allowed. Smaller facets are not allowed because there still could be a coherent reflection from a large one. For the cases analyzed here, the hypothesis appears to be valid.

This hypothesis undoubtedly has limitations. While the partition factor *per se* is not a basis for the establishment of a criterion, it will likely set a small-scale limit to slope

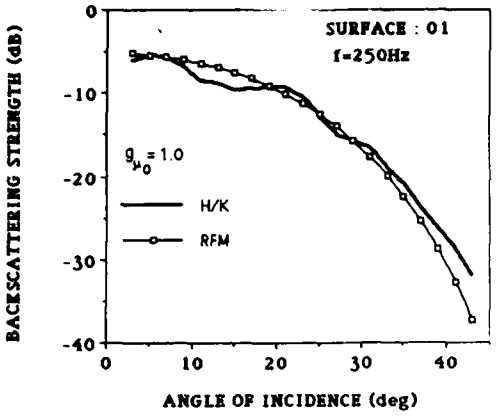

Fig. 7. Comparison of RFM and H/K model results for surface 01 for the best fit at b_{est}=1.85 and $g_{\mu o}$=1.

scattering; that is, the cutoff wavelength cannot be an arbitrarily small fraction of an acoustic wavelength, while allowing $g_{\mu 0}$ to be near unity. Clearly, the scale would be too small for physical optics to apply. That is, we cannot expect the approximations leading to H/K to be violated too seriously. (We are less concerned with minor violations.) Or, if the surface is so smooth that $g_{\mu 0} < 1$ over the full footprint or many Fresnel zones, then we would likely find only coherently reflecting facets.

There are two implications of these results that are worth further note: coherence loss (i.e., $\exp[-g_{\mu 0}]$) due to microroughness is constant and equal to $1/e$ (−4.3 dB), and the previously assumed frequency independence of $F(\cdot)$, as derived in [5], [13], [14], and others, does not hold for power-law spectra. The implicit frequency dependence of $F(\cdot)$ through the slope of the spectrum of the surface and the cutoff wavenumber (K_c) is strong.

Appendix
Derivation of the Rough Facet Model

The $F(\cdot)$ factor in (2) represents scattering due to the fine-scale slopes (δ_f). It is identical to (9.9.14) in Brekhovskikh and Lysanov (B/L) [5] for the high-frequency limit, where they use the symbol V to represent the Rayleigh reflection coefficient (here R_0) and are only concerned with the large-scale slopes (δ) representing regions of stationary phase. This V was taken outside the integral in B/L (9.7.4), with the assumption that the Rayleigh reflection coefficient changed slowly with angle over the integral.

We are also concerned with roughness on the facets, and treat each facet as a scatterer of the form given in B/L (9.8.7). Following the same procedure, we replace V^2 with V_c^2 from B/L (9.8.7), and we get (in our notation)

$$V^2 \rightarrow \exp(-g_\mu) \cdot R_0^2.$$

When this is put into B/L (9.9.14), (2)–(5), are obtained. We have made two additional assumptions: the height's distribution is Gaussian, and $\exp(-g_\mu)$ is also slowly varying with angle over the integral in B/L (9.7.4). In effect, all we are doing is replacing the Rayleigh reflection coefficient for each specular reflection from a facet with the Eckart coherent reflection coefficient times the Rayleigh reflection coefficient.

As already pointed out in a previous work [9], where the rough facet model was introduced, the factor $\exp(-g_\mu)$ can be identified with one of the diffractive corrections in McDaniel's [4] approach to scattering from composite surfaces using the Kirchhoff approximation for both the large and small scales. In that development, the additional approximation mentioned above is also required.

Acknowledgment

The authors thank ONR and the ARSRP Program Manager, Dr. M. Badiey, for sponsoring this work. They also thank R. Meredith of NRL Code 7172 for a thoughtful review of this paper and useful comments.

References

[1] B.F. Kur'yanov, "The scattering of sound at a rough surface with two types of irregularities, " *Sov. Phys. Acoust.*, vol. 8, pp. 252–257, 1963.
[2] S.T. McDaniel and D.A. Gorman, An examination of the composite-roughness scattering model, " *J. Acoust. Soc. Am.*, vol. 73, pp. 1476–1485, 1983.
[3] W. Bachman, "A theoretical model for the backscattering strength of a composite-roughness sea surface," *J. Acoust. Soc. Am.*, vol. 54, pp. 712–716, 1973.
[4] S.T. McDaniel, "Diffractive corrections to the high frequency Kirchhoff approximation," *J. Acoust. Soc. Am.*, vol. 79, pp. 952–957, 1986
[5] L.M. Brekovskikh and Yu. Lysanov, *Fundamentals of Ocean Acoustics.* Berlin: Springer Verlag, 1982.
[6] J.J. Martin, "Sea-surface roughness and acoustic reverberation: An operational model," *J. Acoust. Soc. Am.*, vol. 40, pp. 697–710, 1966.
[7] D.D. Ellis and D.V. Crowe, "Bistatic reverberation calculations using a three-dimensional scattering function," *J. Acoust. Soc. Am.*, vol. 89, pp. 2207–2214, 1991.
[8] J.W. Caruthers, R.J. Sandy, and J.C. Novarini, "Modified bistatic scattering strength model (BISSM2)," Naval Oceanographic and Atmospheric Research Laboratory, NOARL SP 023:200:90, 1990.
[9] J.W. Caruthers and J.C. Novarini, "Modeling bistatic bottom scattering strength including a forward scattering lobe," *IEEE J. Oceanic Eng.*, vol. 18, pp. 100–106, 1993.
[10] J.W. Caruthers and J.C. Novarini, "Modeling swath bathymetry/sidescan sonar image returns," in *Proc. Inst. Acoust..*, St. Albane, 1993, pp. 261–269.
[11] J.W. Caruthers and J.C. Novarini, "Relating acoustics backscatter data to the geomorphology of the Mid-Atlantic ridge," in *Proc. 1993 Symp. Acoustic Reverberation Special Res. Program*, San Diego, CA, Apr. 1993.
[12] K.V. Mackenzie, "Bottom reverberation for 530 and 1030 cps sound in deep water," *J. Acoust. Soc. Am.*, vol. 33, pp. 1498–1503, 1961.
[13] C. Eckart, "The scattering of sound from the sea," *J. Acoust. Soc. Am.*, vol. 25, pp. 566–570, 1953.
[14] P. Beckman and A. Spizzichino, *The Scattering of Electromagnetic Waves From Rough Surfaces.* New York: Pergamon, 1963.
[15] J.W. Caruthers, R.S. Keiffer, and J.C. Novarini, "Near-field acoustic scattering from simulated 2-D, wind driven surfaces," *J. Acoust. Soc. Am.*, vol. 91, pp. 813–822, 1991.
[16] E.I. Thorsos, "Acoustic scattering from a Pierson-Moskowitz sea surface," *J. Acoust. Soc. Am.*, vol. 88, pp. 335–349, 1990.
[17] J.W. Caruthers and J.C. Novarini, "Numerical modeling of randomly rough surfaces with applications to sea surfaces," Tech. Rep. 71-13-T, Dept. Oceanography, Texas A&M Univ., 1971.
[18] J.W. Caruthers and J.C. Novarini, "Simulation of two-dimensional fine-scale geomorphology," *J. Acoust. Soc. Am.*, vol. 92, p. 2302(A), 1992.
[19] D.R. Jackson and D.P. Winebrenner, "Application of the composite roughness model to high-frequency bottom backscattering," *J. Acoust. Soc. Am.*, vol. 79, pp. 1410–1422, 1986.
[20] S.T. McDaniel and D.F. McCammon, "Composite-roughness theory applied to scattering from fetch-limited seas," *J. Acoust. Soc. Am.*, vol. 85, pp. 1712–1719, 1987.

Jorge C. Novarini received the Licenciate degree in physics from the University of Buenos Aires in 1967, and the Sc.D. degree in physics from the same institution in 1972, with thesis work carried out at Texas A&M University.

From 1967 to 1969 he was with the Hydrographic Service of the Argentine Navy, where he started the Underwater Sound Group. From 1969 to 1971 he was on a fellowship doing research at the Oceanography Department of Texas A&M University on numerical modeling of sea surface scattering. From 1972 to 1975 he served as Head of the Underwater Sound Branch of the Hydrographic Service, working on shallow water propagation and acoustical oceanography. From 1976 to 1977 and in 1979 he was an Adjunct Associate Professor at the Physics Department of the Naval Postgraduate School, Monterey, CA, where he worked on numerical modeling of surface scattering. From 1980 to 1991 he served as Head of the Underwater Sound Division of the Service for Naval Research of the Argentine Navy, working on shallow water propagation. During 1983 and 1984 he worked for Ocean Acoustics Associated, Pebble Beach, CA, on numerical modeling of surface scattering and Artic propagation. From 1987 to 1989 he was with Syntek Computer and Engineering, Inc. as a Senior Scientist working on-site at NORDA on surface and bottom scattering. From 1973 to 1986 he was also part-time with the Department of Physics of the University of Buenos Aires, Argentina, where he attained, in 1983, the rank of Professor of Physics. He served also, in 1983, as Secretary for Academic Affairs of the University of Buenos Aires. In 1992 he joined Planning Systems Inc.

Dr. Novarini is member of the Acoustical Society of America and Sigma Xi.

Jerald W. Caruthers received the B.S., M.S., and Ph.D. degrees in physics from Texas A&M University in 1961, 1965, and 1968, respectively.

He began work in ocean science and acoustics as an Assistant Professor of Physical Oceanography in 1968. He has had several management positions at the Naval Ocean Research and Development Activity (NORDA) and the Naval Oceanographic Office (NAVOCEANO). He is presently a Research Physicist at the Naval Research Laboratory (NRL) at Stennis Space Center, MS.